Supporting Information

Uncovering the Untapped Potentials of Copper(I) Sulphide toward Lithium-Ion Storage under Ultra-Low Temperatures

Yifan Chen [a], Jinze Wang [b], Youran Hong [c], Yusi Yang [a], Lulu Tan [d], Nan Li [a], Can Ma [a], Jiangwei Wang [c,e], Xiulin Fan [b], and Yujie Zhu *[a,f]

[a] *School of Chemistry, Beihang University, Beijing 100191, China.*

[b] *State Key Laboratory of Silicon Materials, School of Materials Science and Engineering, Zhejiang University, Hangzhou 310027, China.*

[c] *Center of Electron Microscopy and State Key Laboratory of Silicon Materials, School of Materials Science and Engineering, Zhejiang University, Hangzhou 310027, China.*

[d] *School of Physics, Beihang University, Beijing 100191, China.*

[e] *Wenzhou Key Laboratory of Novel Optoelectronic and Nano Materials, Institute of Wenzhou, Zhejiang University, Wenzhou 325006, China.*

[f] *Beijing Advanced Innovation Center for Biomedical Engineering, Beihang University, Beijing 100191, China.*

*Corresponding authors: yujiezhu@buaa.edu.cn (Y. Zhu).

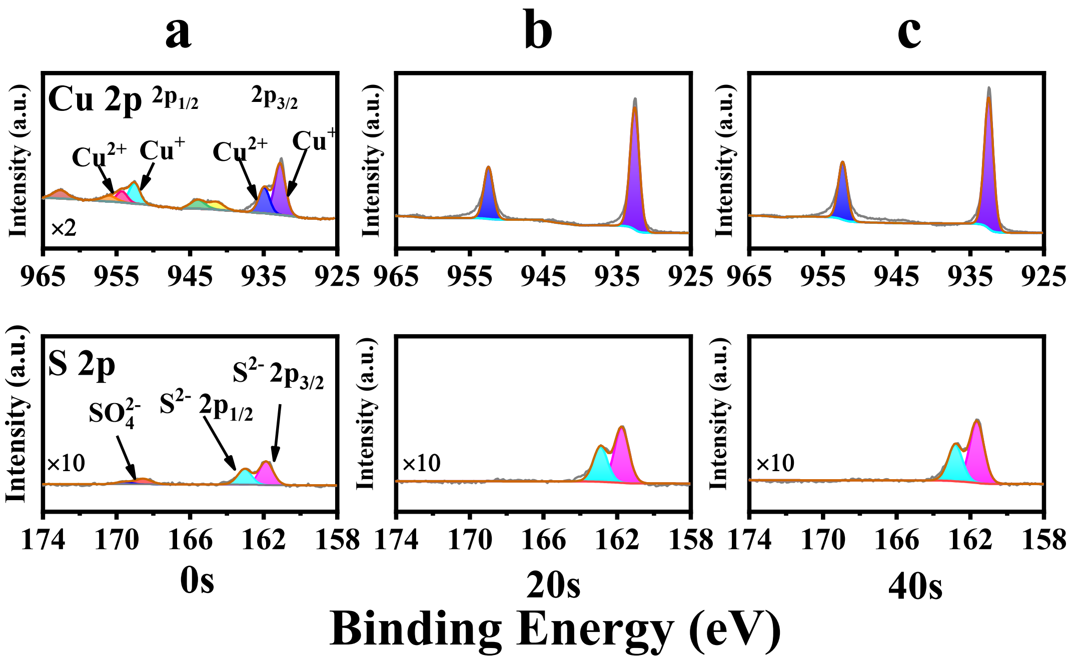

Fig. S1 X-ray photoelectron spectroscopy (XPS) depth-profiling analysis of pristine Cu_2S sample. The Cu 2p (top row) and S 2p (bottom row) spectra after argon ion sputtering for (a) 0 s, (b) 20 s, and (c) 40 s, respectively.

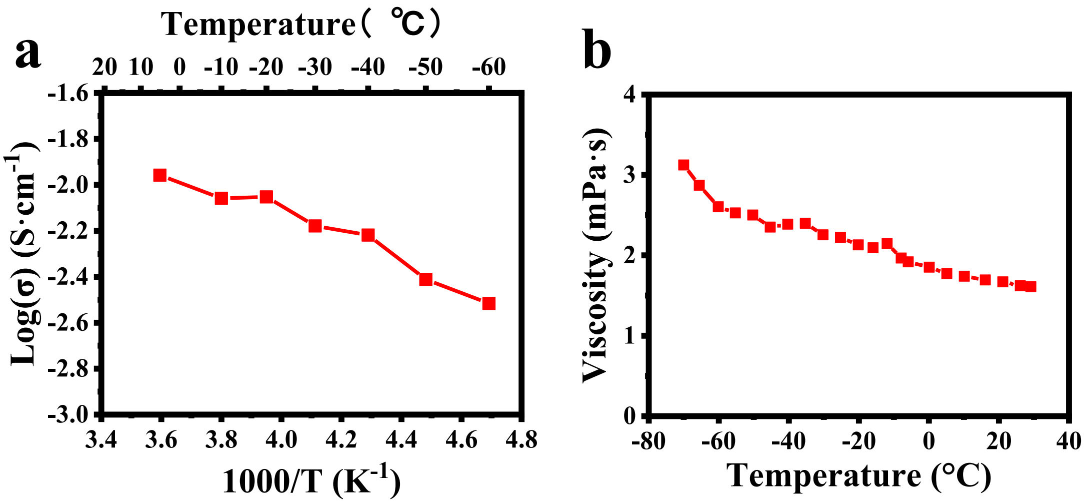

Fig. S2 Physical properties of the 1 M LiTFSI-DOL/DME electrolyte. Temperature dependence of the (a) ionic conductivity and (b) viscosity of the electrolyte.

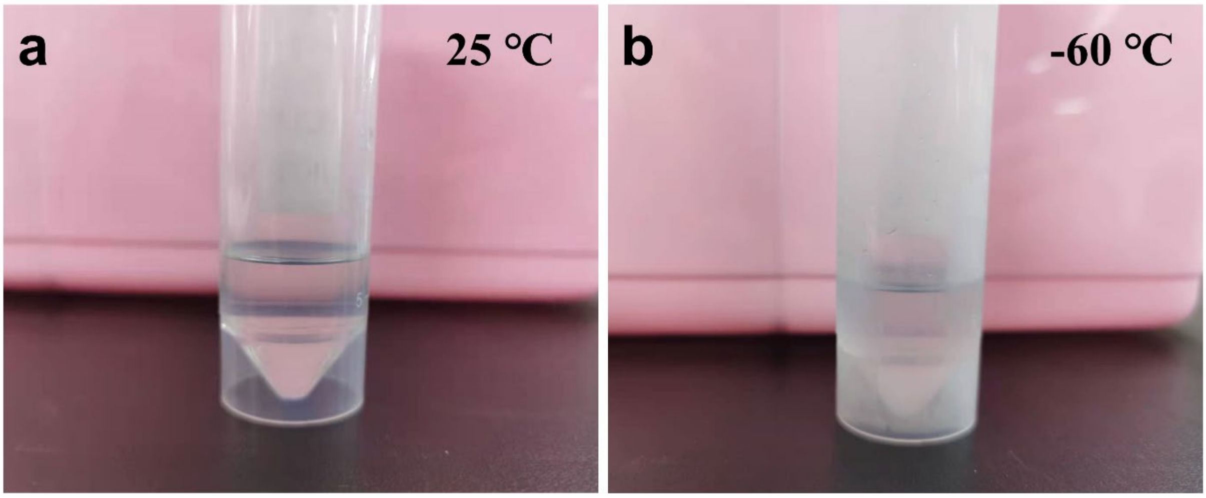

Fig. S3 Digital photos of the 1 M LiTFSI-DOL/DME electrolyte at (a) 25 °C and (b) -60 °C.

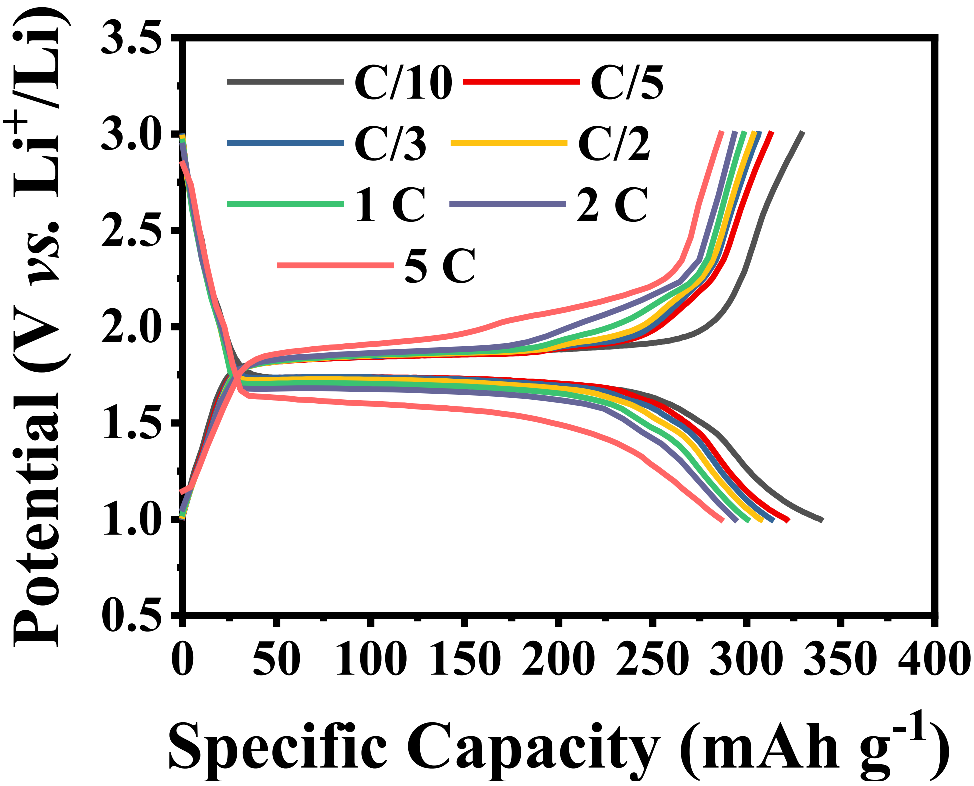

Fig. S4 The galvanostatic charge-discharge curves from 0.1 C to 5 C for the Li-Cu_2S half-cell (with Cu_2S loading of 2.3 mg cm^{-2}) under 25 °C.

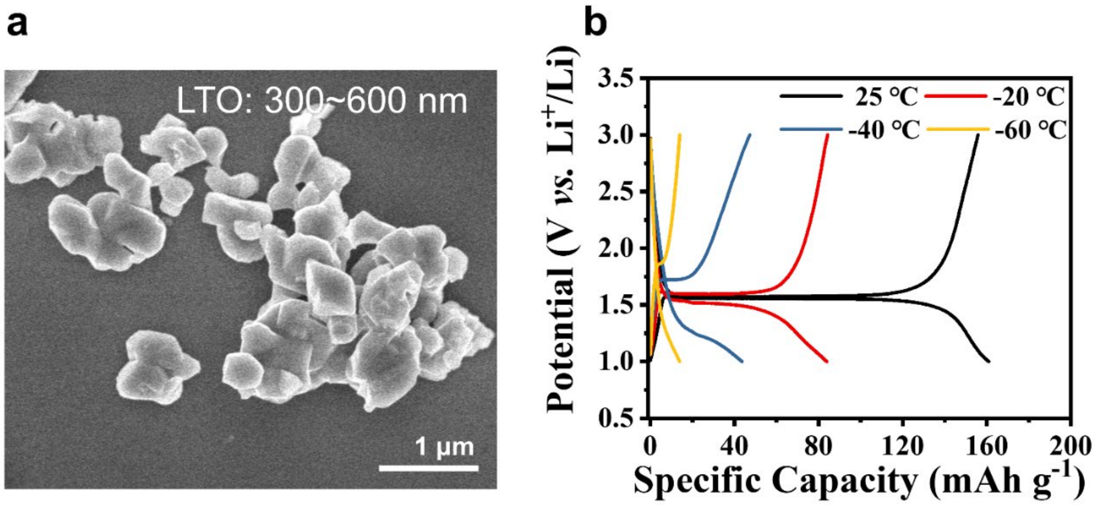

Fig. S5 (a) The SEM image of commercial LTO powder and (b) the galvanostatic charge-discharge potential profiles of LTO coated on Cu foil current collector at 25 °C, -20 °C, -40 °C, and -60 °C. The charge-discharge current rate and mass loading of LTO in (b) is 0.2 C (32 mA g^{-1}) and 2.1 mg cm^{-2}.

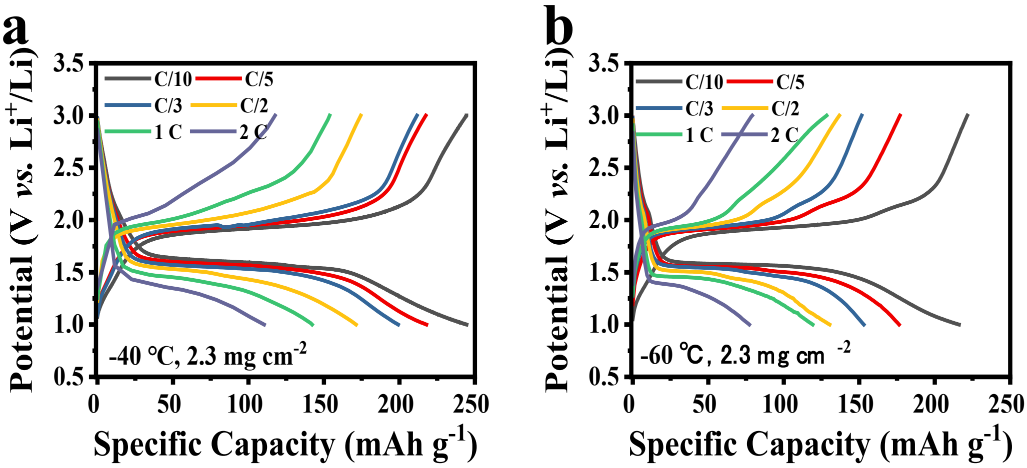

Fig. S6 The galvanostatic charge-discharge curves from 0.1 C (33 mA g^{-1}) to 2 C (674 mA g^{-1}) for the Li-Cu_2S half-cells (with Cu_2S loading of 2.3 mg cm^{-2}) at (a) -40 °C and (b) -60 °C.

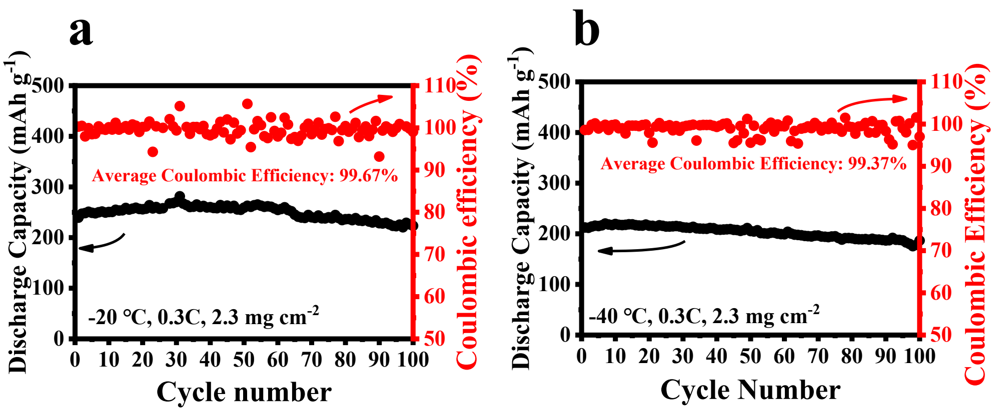

Fig. S7 Cycling performance of the Li-Cu_2S half-cells (with Cu_2S loading of 2.3 mg cm^{-2}) at 0.3 C (100 mA g^{-1}) under (a) -20 °C and (b) -40 °C.

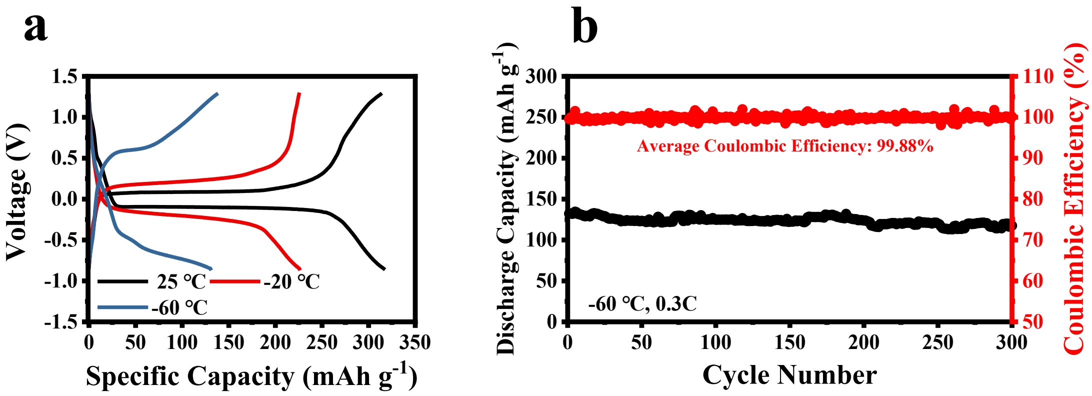

Fig. S8 (a) The galvanostatic charge-discharge curves of the Cu_2S-Cu_2S symmetrical cell tested at 0.3 C (100 mA g^{-1}) under 25, -20, and -60 °C. (b) Cycling performance of the Cu_2S-Cu_2S symmetrical cell tested at 0.3 C (100 mA g^{-1}) under -60 °C.

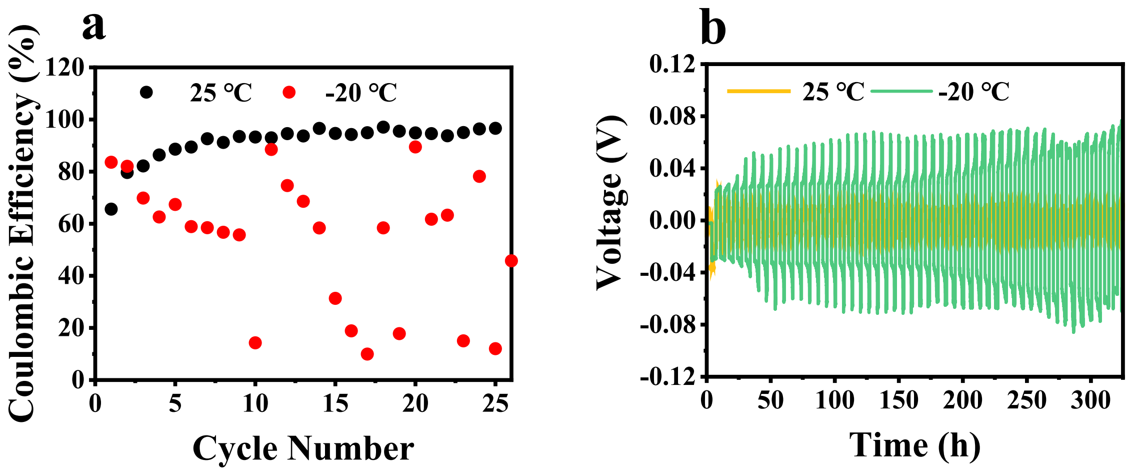

Fig. S9 (a) The Li plating-stripping Coulombic efficiency (under a plating capacity of 0.8 mAh cm^{-2}) measured in the Li-Cu cell at 0.23 mA cm^{-2} (equal to the areal current density used in Fig. 2c，2.3 mg cm^{-2} × 100 mA g^{-1}) under 25 and -20 °C. (b) Voltage profiles of the Li-Li symmetrical cell tested at 25 and -20 °C with a current density of 0.23 mA cm^{-2} and areal capacity of 0.8 mAh cm^{-2}.

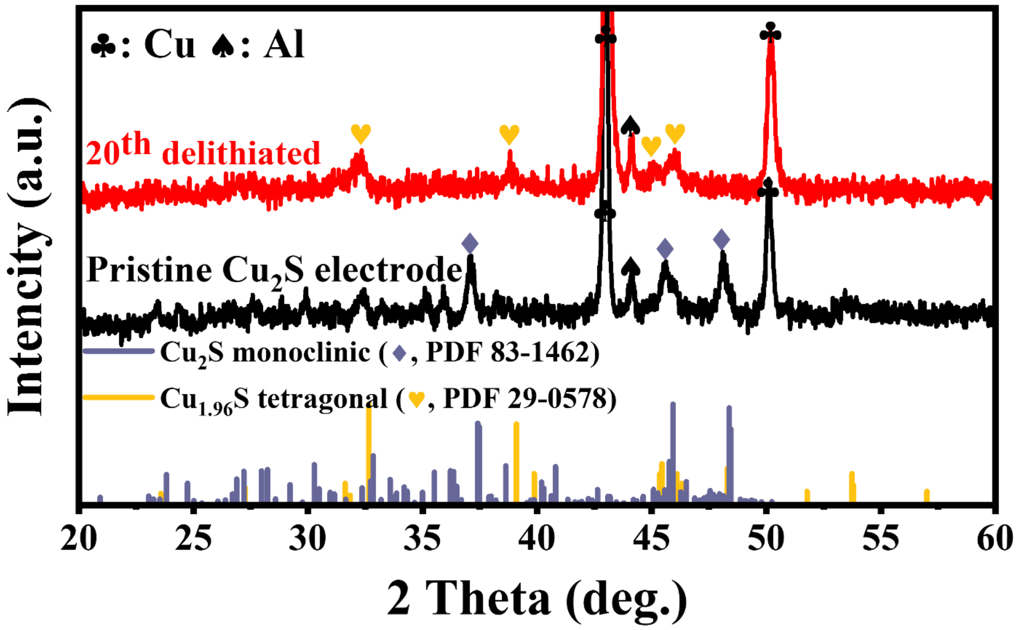

Fig. S10 XRD patterns of pristine Cu_2S electrode (with Cu foil as the current collector) (black line) and the one after the 20th delithiation at 0.3 C (red line) with the standard diffraction patterns of monoclinic Cu_2S (JCPDF No. 83-1462) and tetragonal $Cu_{1.96}S$ (JCPDF No. 29-0578) also presented. Note: the Al signals originate from the aluminium XRD sample holder.

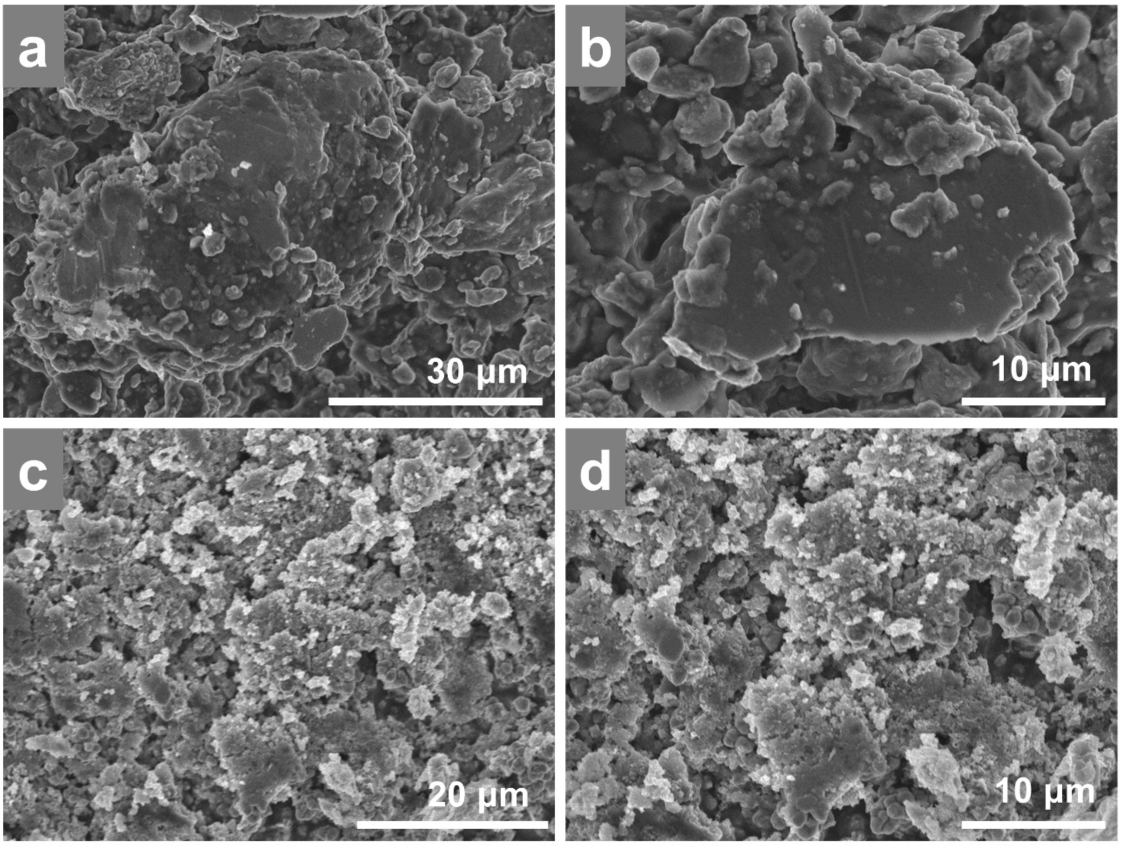

Fig. S11 SEM images of (a, b) pristine Cu_2S electrode (with Cu foil as the current collector) and (c, d) the one after the 20th delithiation at 0.3 C.

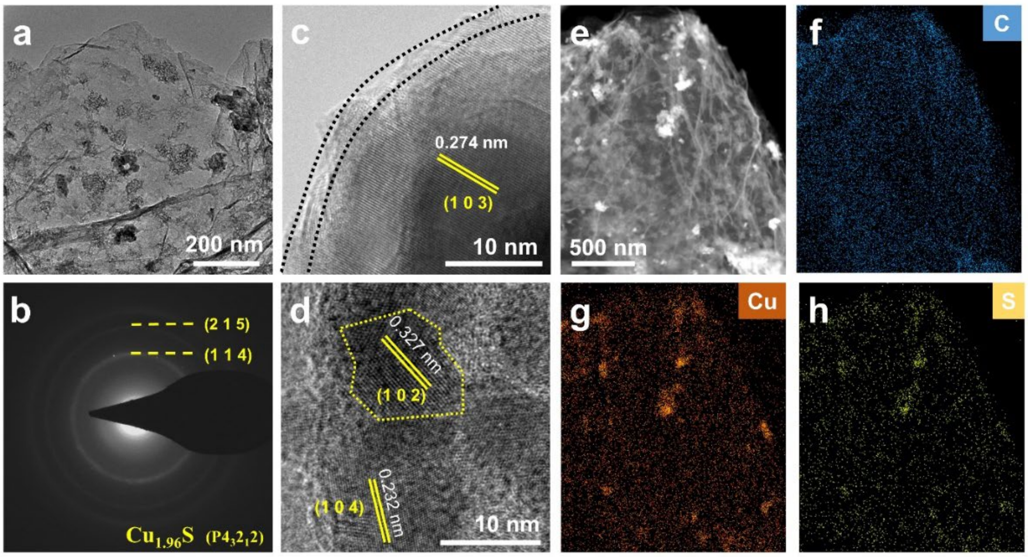

Fig. S12 Post-mortem TEM characterizations of the Cu_2S after the 20th delithiation at 0.3 C. (a) The TEM image, (b) SAED pattern, (c-d) HRTEM images (with the *d*-spacings of crystal planes of $Cu_{1.96}S$ marked), and (e-h) elements mapping results ((f) C, (g) Cu, and (h) S) of the sample.

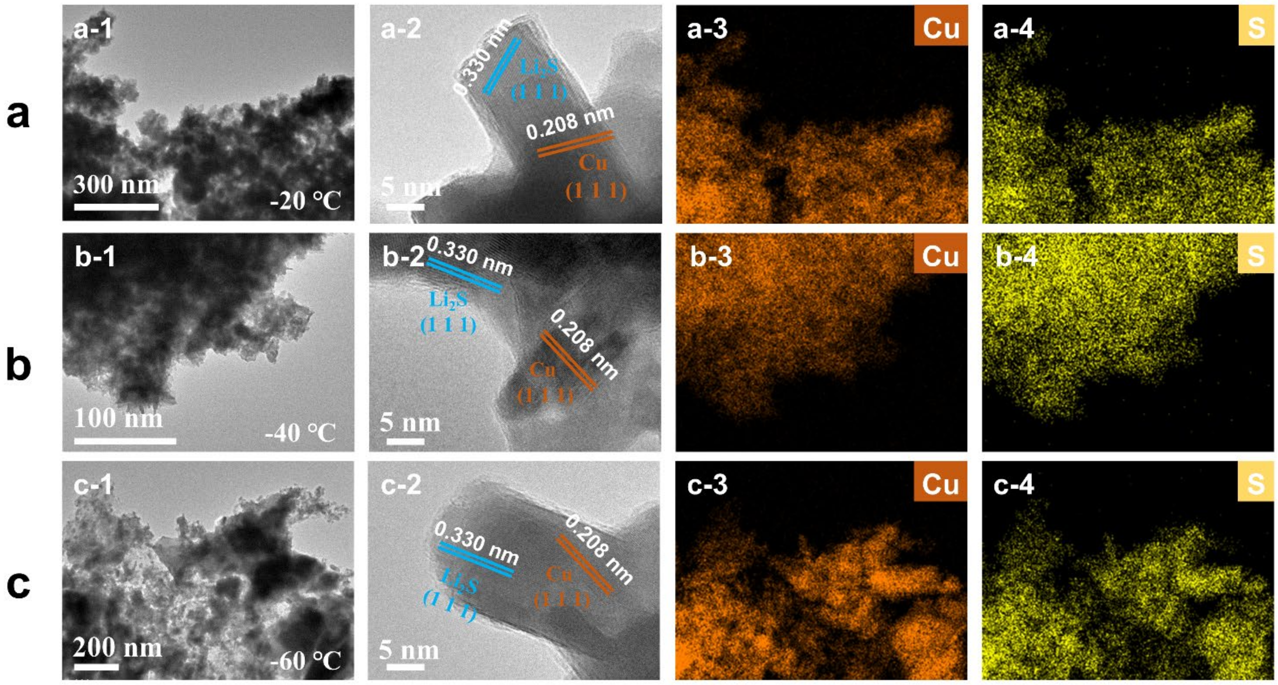

Fig. S13 (a-1, b-1, c-1) TEM and (a-2, b-2, c-2) HRTEM images (with the *d*-spacings of crystal planes of Li_2S and Cu marked) of the Cu_2S electrode after the 10^{th} lithiation at 0.3 C under (a) -20, (b) -40, and (c) -60 °C. The corresponding Cu (a-3, b-3, c-3) and S (a-4, b-4, c-4) elemental mapping results of the lithiated samples.

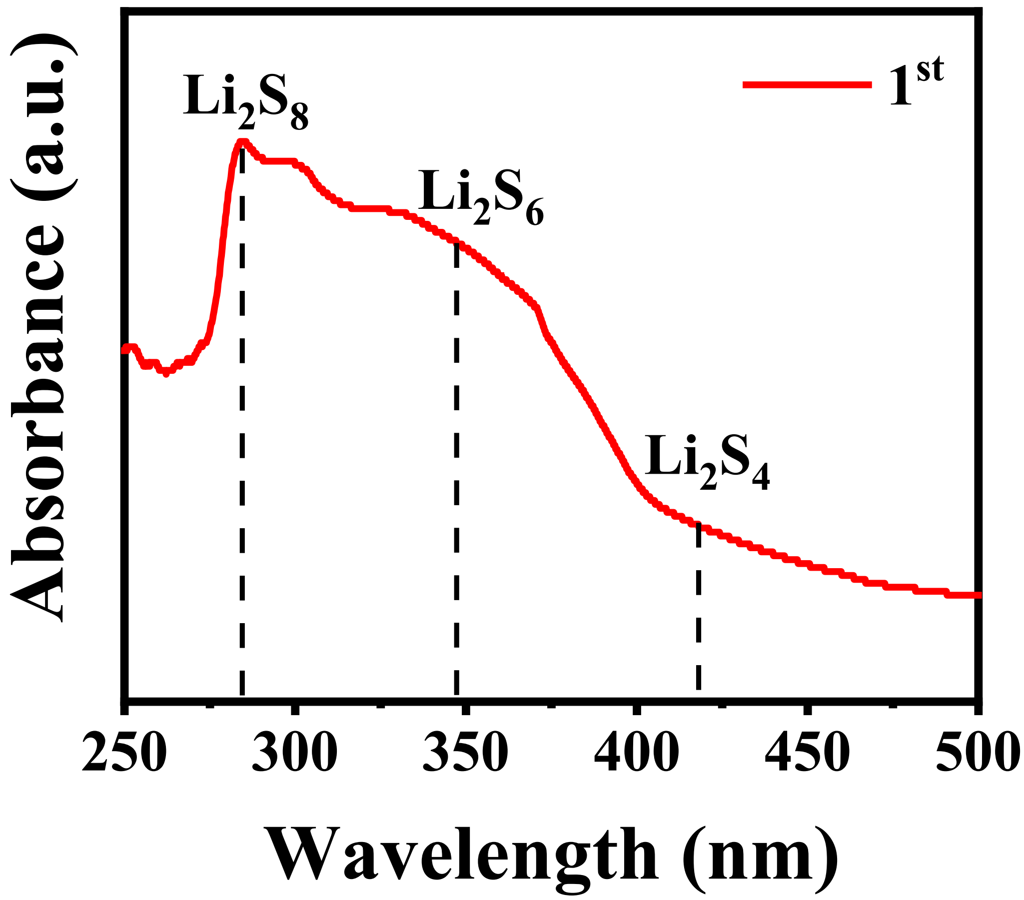

Fig. S14 UV-vis absorbance spectra (red line) of the electrolyte which was retrieved from the Li-Cu_2S cells after the first lithiation-delithiation cycle. The characteristic signals (dashed lines) of Li_2S_8, Li_2S_6, and Li_2S_4 are also marked.

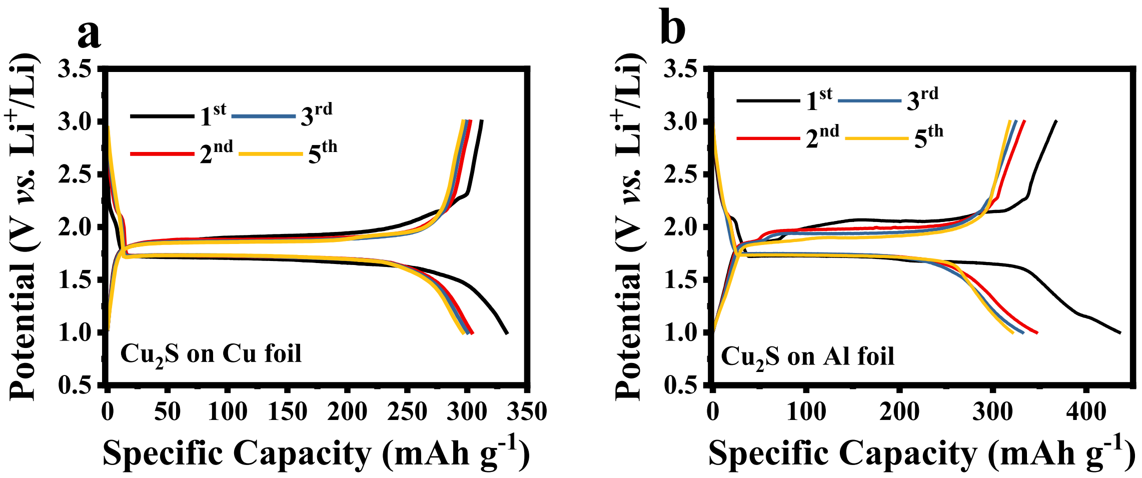

Fig. S15 The galvanostatic charge-discharge potential profiles of the Li-Cu_2S half-cells with Cu_2S coated on the (a) Cu and (b) Al foil, respectively. The results clearly show the absence of the 2.28 V delithiation plateau.

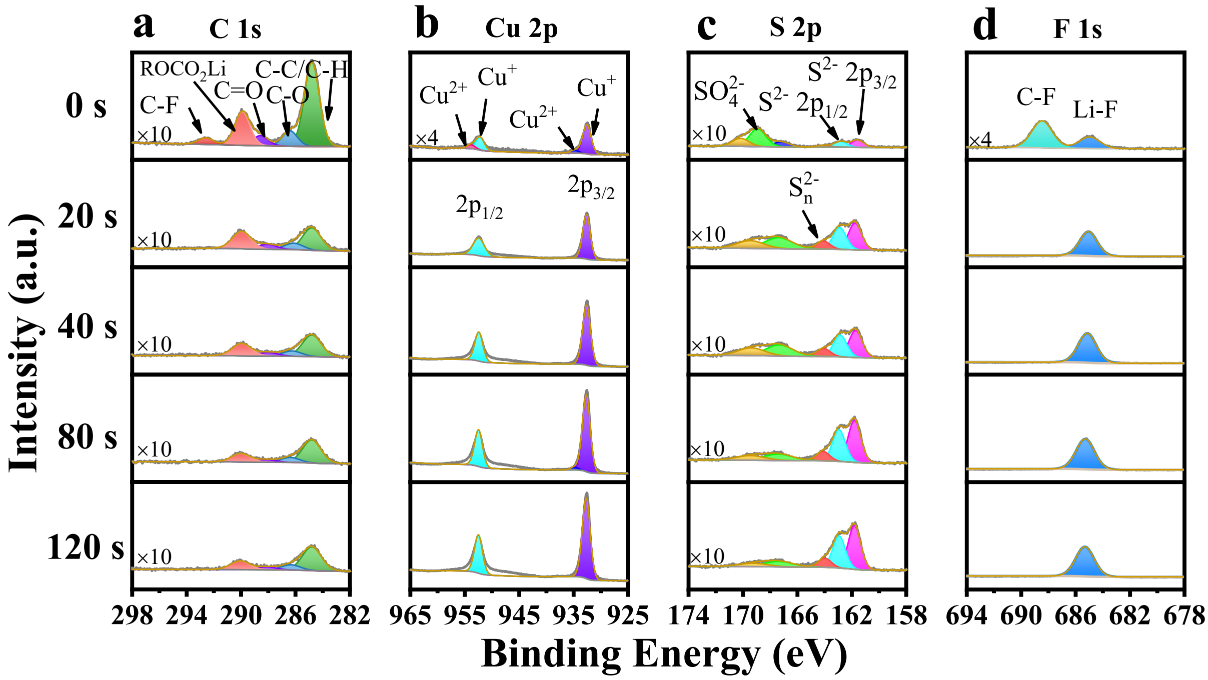

Fig. S16 XPS depth-profiling analysis of the delithiated Cu_2S electrode after 50 cycles at 0.3 C. The (a) C 1s, (b) Cu 2p, (c) S 2p, and (d) F 1s spectra after argon ion sputtering for 0 s, 20 s, 40 s, 80 s, and 120 s, respectively.

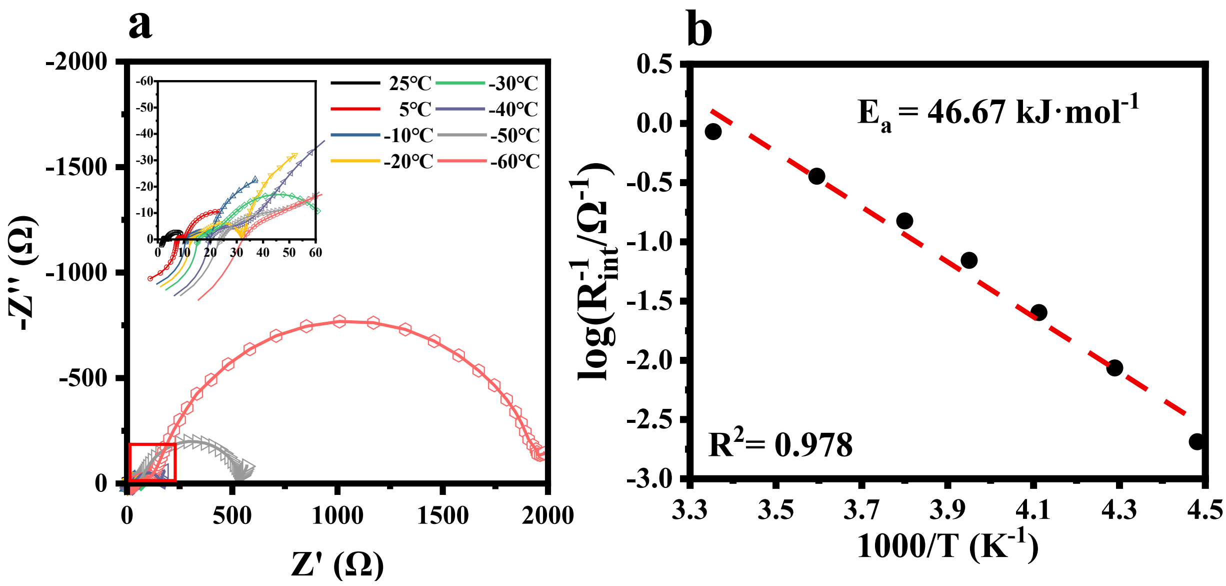

Fig. S17 (a) The Nyquist plots of the Li-Li symmetric cell at different temperatures. The inset: the enlarged view of the part marked by the red square. (b) The interfacial resistance R_{int} fitted by the Arrhenius equation to obtain the activation energy E_a.

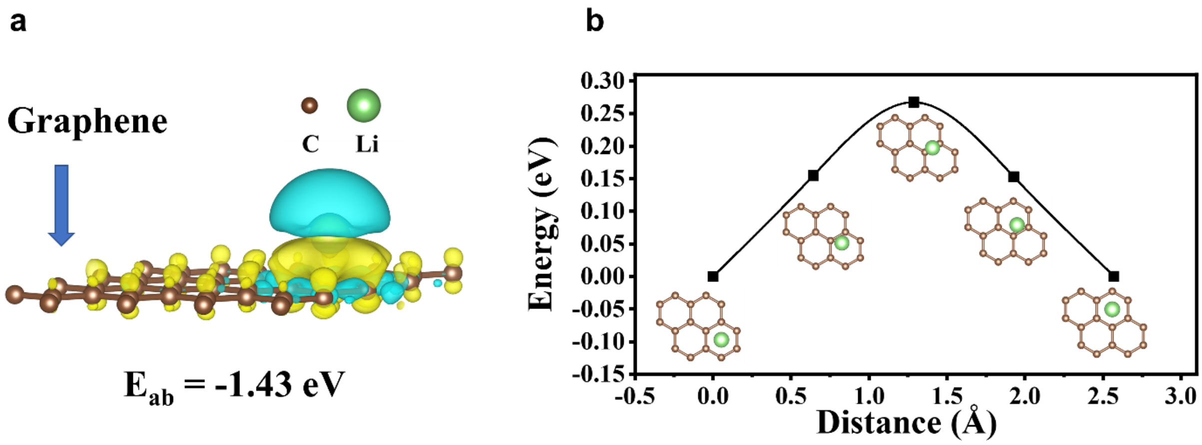

Fig. S18 (a) The calculated charge density difference and adsorption energy of Li-ion adsorbed on the graphene surface (yellow: charge increase, blue: charge decrease). (b) The calculated energy barrier for the Li-ion diffusion on the surface of graphene (the insets show the configurations of the Li-ion at various states during the diffusion process).

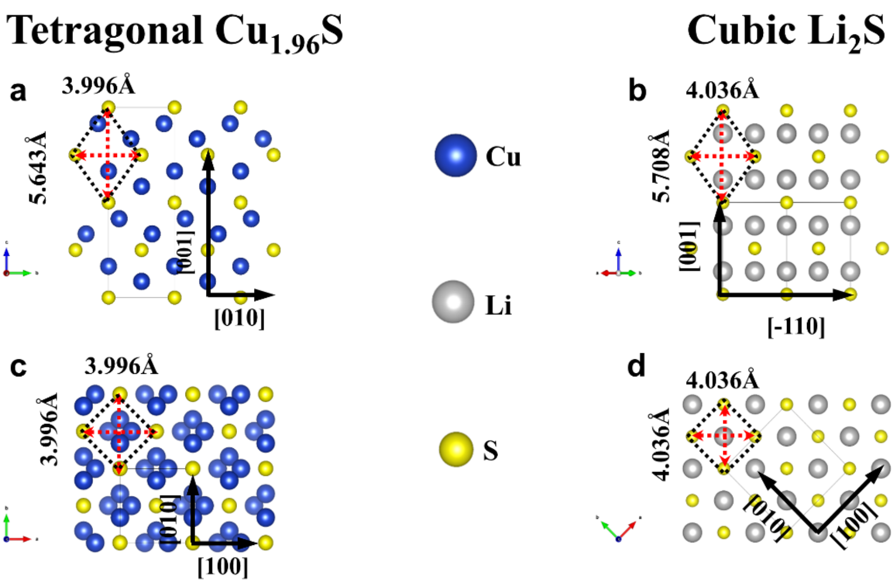

Fig. S19 Structure of tetragonal $Cu_{1.96}S$ along the (a) [100] and (c) [001] directions versus cubic Li_2S along the (b) [110] and (d) [001] directions. Rhombic and square shapes mark the networks formed by sulfur atoms.

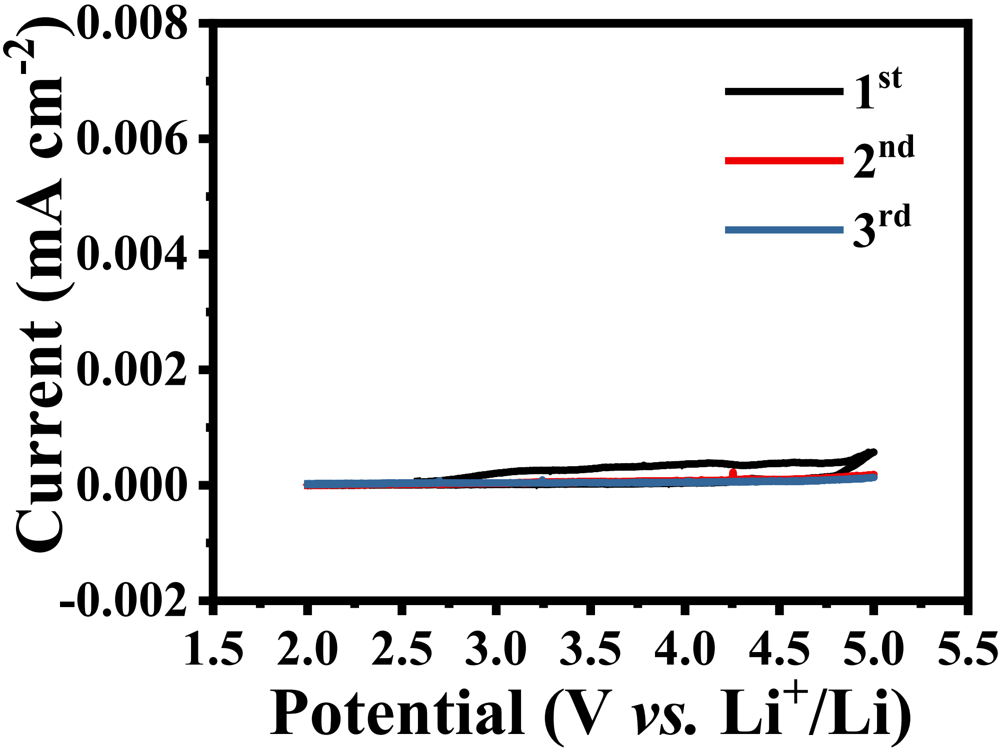

Fig. S20 Cyclic voltammograms of the 1 M LiTFSI-DOL/DME electrolyte between 2.0 and 5.0 V (*vs.* Li^+/Li), which are obtained with Al foil as the working electrode and lithium metal as the counter and reference electrode. The scan rate is 0.1 mV s^{-1}.

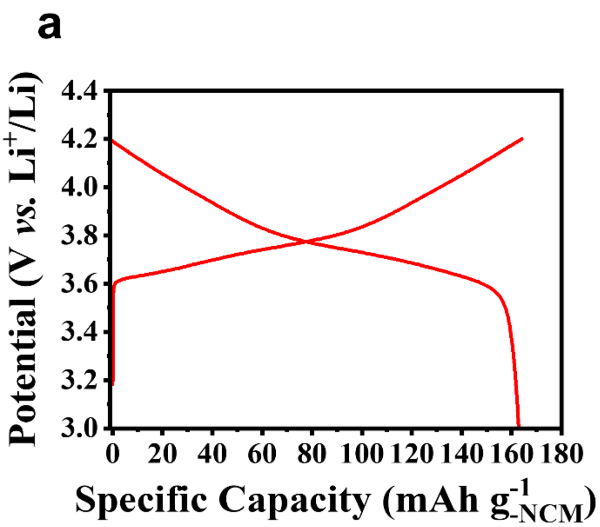

Fig. S21 (a) The galvanostatic charge-discharge potential profiles and (b) cycling performance of the Li-NCM half-cell under a current rate of 0.1 C (1C = 160 mA g^{-1}) and 25 °C.

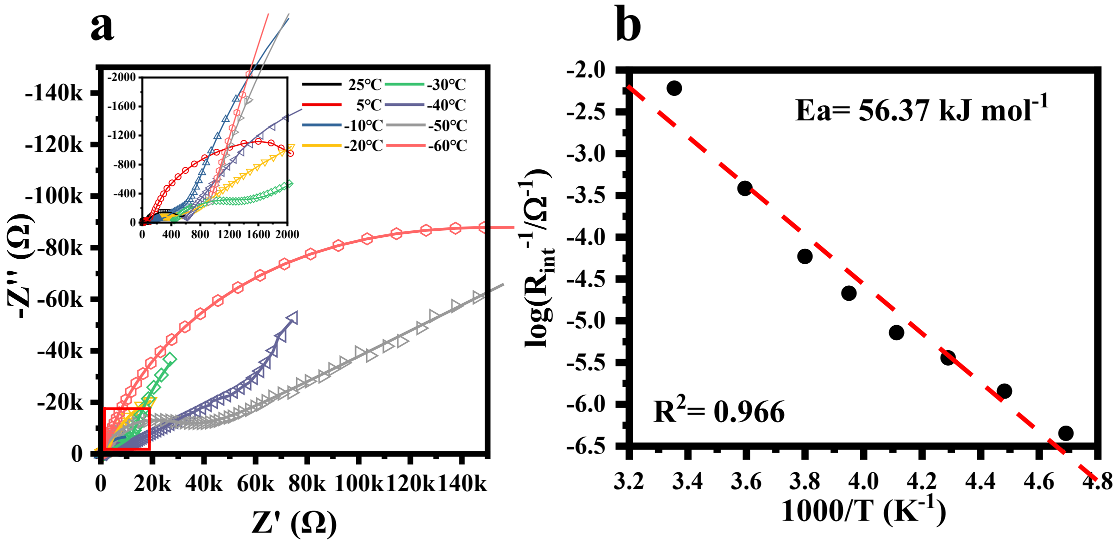

Fig. S22 (a)The Nyquist plots of the NCM-NCM symmetric cell at different temperatures. The inset: the enlarged view of the part marked by the red square. (b) The interfacial resistance R_{int} fitted by the Arrhenius equation to obtain the activation energy E_a.

Table S1 A comparison of the low-temperature electrochemical performances between this work and other reported anode materials.

Material	Current Density	Specific Capacity (mAh g^{-1})	Areal Capacity (mAh cm^{-2})	Cycles	Article
Cu_2S powder	**0.3 C**	**316.6(25 °C), 268(-20 °C), 229(-40 °C), 182(-60 °C)**	**2.09(25 °C, 0.1 C), 1.56(-20°C, 0.1 C), 1.31(-40 °C, 0.1 C)**	**180(-40 °C, 0.3 C), 350(-60 °C, 0.3 C)**	**This work**
Graphite + Cu powder	0.3 C	364(20 °C), 290(-10 °C), 208(-20 °C), 130(-30 °C)	0.73(20 °C), 0.58(-10 °C), 0.42(-20 °C), 0.26(-30 °C)	NA	1
Graphite + Cu layer	0.3 C	372(20 °C), 294(-10 °C), 156(-20 °C), 103(-30 °C)	0.74(20 °C), 0.59(-10 °C), 0.31(-20 °C), 0.21(-30 °C)	NA	1
Graphite + Sn powder	0.2 C	370(20 °C), 299(-10 °C), 226(-20 °C), 94(-30 °C)	1.11(20 °C), 0.897(-10 °C), 0.68(-20 °C), 0.28(-30 °C)	NA	2
Graphite + Sn layer	0.2 C	377(20 °C), 342(-10 °C), 273(-20 °C), 152(-30 °C)	1.13(20 °C), 1.03(-10 °C), 0.82(-20 °C), 0.46(-30 °C)	NA	2
EMCMB	0.2 C	376(20 °C), 100(-40 °C)	NA	NA	3
Graphite + Cu/Super-P	0.2 C	372(20 °C), 340(-10 °C), 280(-20 °C), 178(-30 °C)	0.93(20 °C), 0.85(-10 °C), 0.70(-20 °C), 0.45(-30 °C)	100(-30 °C, 0.2 C)	4
GRAL	0.05 C	345(20 °C), 215(-20 °C), 130(-30 °C)	0.26(20 °C), 0.16(-20 °C), 0.10(-30 °C)	50(-20 °C and -30 °C,0.15 C)	5
CG-1000, FWNT	0.037C	341(20 °C), 300(0 °C), 215 (-20 °C), 154(-40 °C), 52(-60 °C)	NA	100(-40 °C, 0.037C)	6
PGN/CNT	0.1C	372(20 °C), 330(-10 °C), 300(-20 °C), 180(-40 °C)	0.74(20 °C), 0.66(-10 °C), 0.60(-20 °C), 0.36(-40 °C)	NA	7
350nm LTO	0.125C	152(20 °C), 135(-10 °C), 115(-20 °C), 83(-30 °C)	0.32(20 °C), 0.28(-10 °C), 0.24(-20 °C), 0.17(-30 °C)	NA	8
700nm LTO	0.125C	162(20 °C), 92(-10 °C), 60(-20 °C), 35(-30 °C)	0.34(20 °C), 0.19(-10 °C), 0.13(-20 °C), 0.07(-30 °C)	NA	8
LTO + Cu/Super -P	0.2C	157(20 °C), 150(-10 °C), 142(-20 °C), 131(-30 °C)	0.39(20 °C), 0.37(-10 °C), 0.35(-20 °C), 0.33(-30 °C)	NA	9
La^{3+}, F^- LTO	1C, 5C	135(0 °C), 120(-10 °C), 100(-20 °C)	NA	100(-20 °C, 1 C)	10
$Li_{3.9}Cr_{0.3}Ti_{4.8}O_{12}$	1C	166(25 °C), 129(-10 °C), 100(-20 °C)	0.16(25 °C), 0.12(-10 °C), 0.1(-20 °C)	100 (-10 °C, 1 C)	11
NH_4F-modified LTO	1C	175(25 °C), 130(-10 °C), 100(-20 °C)	0.19(25 °C), 0.14(-10 °C), 0.11(-20 °C)	NA	12

LTO/HCMS-C	1C	138(25 °C), 113(-10 °C), 107(-20 °C), 96(-30 °C)	NA	100(-20 °C, 10C)	13
HP LTO-TO microspheres	0.2C	163(25 °C), 135.6(-10 °C), 129.8(-20 °C), 118.5(-30 °C), 93.6(-40 °C)	0.18(25 °C), 0.153(-10 °C), 0.147(-20 °C), 0.134(-30 °C), 0.106(-40 °C)	50(-20 °C, 0.2C)	14
Li_3VO_4/C	0.2C	550(25 °C), 200(-20 °C)	1.10(25 °C), 0.4(-20 °C)	80(-20 °C, 1 C)	15
Nb_2O_5	0.5C	188(25 °C), 95(-75 °C)	0.19(25 °C), 0.09(-75 °C)	100(-75 °C, 0.5 C)	16
Sn-PMCMT	0.25C	610(20 °C), 190(-20 °C)	0.61(20 °C), 0.19(-20 °C)	NA	17
SnO_2	0.13C	901.5(30 °C), 780.7(-10 °C), 666.7(-20 °C), 342.8(-30 °C)	NA	100(-30°C, 0.13 C)	18
Ge (ZnRR)	0.5C	1200(25 °C), 566(- 20°C)	NA	50(-20 °C, 0.5 C)	19
$GeO_{1.57}$@Ti_3C_2 Mxene	0.2C	1127(25 °C), 711.4(-20 °C), 298.3(-40°C)	1.13(25 °C), 0.711(-20 °C), 0.298(-40 °C)	100(-40 °C, 0.2 C)	20
Ge NWs	1C	1590(20 °C), 1100(-20 °C), 750(-30 °C), 480(-40 °C), 225(-50 °C)	0.09(20 °C), 0.06(-20 °C), 0.04(-30 °C), 0.03(-40 °C), 0.01(-50 °C)	NA	21
$Cu_{18}Zn_{82}$	0.3C	300(20 °C), 238(-10 °C), 197(-20 °C), 137(-30 °C)	0.90(20 °C), 0.714(-10 °C), 0.591(-20 °C), 0.411(-30 °C)	200(-10 °C, 0.3 C)	22
ZnS/C(9.3wt%)	1C	360(20 °C), 207(-20 °C)	NA	50(-20 °C,1 C)	23
MnO@Graphite	0.1C	1000(20 °C), 456(-25 °C)	NA	320(-25 °C,0.1 C)	24
Ag–Fe_2O_3/CNF	0.5C	830(20 °C), 560(-5 °C)	1.24(20 °C), 0.84(-5 °C)	65(-5°C, 0.5 C)	25
Fe_3O_4@NCm	0.2C	1607(20 °C), 1070(-20 °C)	1.61(20 °C), 1.07(-20 °C)	900(-20 °C, 0.2 C)	26
MoS_2/graphite	0.1C	1028(25 °C), 720(-20 °C)	NA	40(-20 °C, 0.5 C)	27
MoS_2 nanosheets	0.1C	1200(25 °C), 775(-20 °C)	1.80(20 °C), 1.16(-20 °C)	50(-20 °C, 0.1 C)	28
Co_3O_4@graphene	0.2C	920(30 °C), 730.8(-10 °C), 593.6(-20 °C), 537.5(-30 °C)	0.92(30 °C), 0.73(-10 °C), 0.59(-20 °C), 0.54(-30 °C)	600(-10 °C, 0.2 C)	29
Peony-like holey Co_3O_4	0.2C	1883(25 °C), 642(-25 °C)	1.88(25 °C), 0.642(-25 °C)	50(-25 °C,0.2 C)	30
NiO@C-N nanosheets	0.05C	1036(25 °C), 800(-25 °C), 428(-40 °C)	0.52(25 °C), 0.4(-25 °C), 0.216(-40 °C)	NA	31

Reference

1 M. Mancini, F. Nobili, S. Dsoke, F. D'Amico, R. Tossici, F. Croce and R. Marassi, *J. Power Sources*, 2009, **190**, 141-148.
2 F. Nobili, M. Mancini, S. Dsoke, R. Tossici and R. Marassi, *J. Power Sources*, 2010, **195**, 7090-7097.

3 G. Zhao, Z. Wei, N. Zhang and K. Sun, *Mater. Lett.*, 2012, **89**, 243-246.
4 M. Marinaro, M. Mancini, F. Nobili, R. Tossici, L. Damen and R. Marassi, *J. Power Sources*, 2013, **222**, 66-71.
5 R. Raccichini, A. Varzi, V. S. K. Chakravadhanula, C. Kübel, A. Balducci and S. Passerini, *J. Power Sources*, 2015, **281**, 318-325.
6 M. J. Lee, K. Lee, J. Lim, M. Li, S. Noda, S. J. Kwon, B. DeMattia, B. Lee and S. W. Lee, *Adv. Funct. Mater.*, 2021, **31**, 2009397.
7 J. Xu, X. Wang, N. Yuan, B. Hu, J. Ding and S. Ge, *J. Power Sources*, 2019, **430**, 74-79.
8 J. L. Allen, T. R. Jow and J. Wolfenstine, *J. Power Sources*, 2006, **159**, 1340-1345.
9 M. Marinaro, F. Nobili, A. Birrozzi, S. K. Eswara Moorthy, U. Kaiser, R. Tossici and R. Marassi, *Electrochim. Acta*, 2013, **109**, 207-213.
10 M. Ji, Y. Xu, Z. Zhao, H. Zhang, D. Liu, C. Zhao, X. Qian and C. Zhao, *J. Power Sources*, 2014, **263**, 296-303.
11 H. L. Zou, H. F. Xiang, X. Liang, X. Y. Feng, S. Cheng, Y. Jin and C. H. Chen, *J. Alloys Compd.*, 2017, **701**, 99-106.
12 Y. Zhang, Y. Luo, Y. Chen, T. Lu, L. Yan, X. Cui and J. Xie, *ACS Appl. Mater. Interfaces*, 2017, **9**, 17145-17154.
13 C.-K. Ho, C.-Y. V. Li, Z. Deng, K.-Y. Chan, H. Yung and C. Yang, *Carbon*, 2019, **145**, 614-621.
14 C. Huang, S.-X. Zhao, H. Peng, Y.-H. Lin, C.-W. Nan and G.-Z. Cao, *J. Mater. Chem. A*, 2018, **6**, 14339-14351.
15 Z. Liang, Y. Zhao, Y. Dong, Q. Kuang, X. Lin, X. Liu and D. Yan, *J. Electroanal. Chem.*, 2015, **745**, 1-7.
16 X. Dong, Y. Yang, P. Li, Z. Fang, Y. Wang and Y. Xia, *Batteries Supercaps*, 2020, **3**, 1016-1020.
17 F. Nobili, I. Meschini, M. Mancini, R. Tossici, R. Marassi and F. Croce, *Electrochim. Acta*, 2013, **107**, 85-92.
18 L. Tan, R. Hu, H. Zhang, X. Lan, J. Liu, H. Wang, B. Yuan and M. Zhu, *Energy Storage Mater.*, 2021, **36**, 242-250.
19 S. Choi, Y.-G. Cho, J. Kim, N.-S. Choi, H.-K. Song, G. Wang and S. Park, *Small*, 2017, **13**, 1603045.
20 M. Shang, X. Chen, B. Li and J. Niu, *ACS Nano*, 2020, **14**, 3678-3686.
21 I. M. Gavrilin, Y. O. Kudryashova, A. A. Kuz'mina, T. L. Kulova, A. M. Skundin, V. V. Emets, R. L. Volkov, A. A. Dronov, N. I. Borgardt and S. A. Gavrilov, *J. Electroanal. Chem.*, 2021, **888**, 115209.
22 A. Varzi, L. Mattarozzi, S. Cattarin, P. Guerriero and S. Passerini, *Adv. Energy Mater.*, 2018, **8**, 1701706.
23 L. He, X.-Z. Liao, K. Yang, Y.-S. He, W. Wen and Z.-F. Ma, *Electrochim. Acta*, 2011, **56**, 1213-1218.
24 X. Tian, L. Du, Y. Yan and S. Wu, *ChemElectroChem*, 2019, **6**, 2248-2253.
25 M. Zou, J. Li, W. Wen, L. Chen, L. Guan, H. Lai and Z. Huang, *J. Power Sources*, 2014, **270**, 468-474.
26 Q. Chen, W. Zhong, J. Zhang, C. Gao, W. Liu, G. Li and M. Ren, *J. Alloys Compd.*, 2019, **772**, 557-564.
27 Y. Teng, H. Zhao, Z. Zhang, Z. Li, Q. Xia, Y. Zhang, L. Zhao, X. Du, Z. Du, P. Lv and K. Świerczek, *ACS Nano*, 2016, **10**, 8526-8535.
28 X. Liu, Y. Wang, Y. Yang, W. Lv, G. Lian, D. Golberg, X. Wang, X. Zhao and Y. Ding, *Nano Energy*, 2020, **70**, 104550.
29 L. Tan, X. Lan, R. Hu, J. Liu, B. Yuan and M. Zhu, *ChemNanoMat*, 2021, **7**, 61-70.
30 H. Duan, L. Du, S. Zhang, Z. Chen and S. Wu, *J. Mater. Chem. A*, 2019, **7**, 8327-8334.
31 Z. Bai, X. Lv, D.-H. Liu, D. Dai, J. Gu, L. Yang and Z. Chen, *ChemElectroChem*, 2020, **7**, 3616-3622.